ADVANCED FUNCTIONAL MATERIALS
www.afm-journal.de

Stretchable-Rubber-Based Triboelectric Nanogenerator and Its Application as Self-Powered Body Motion Sensors

Fang Yi, Long Lin, Simiao Niu, Po Kang Yang, Zhaona Wang, Jun Chen, Yusheng Zhou, Yunlong Zi, Jie Wang, Qingliang Liao, Yue Zhang, and Zhong Lin Wang**

A stretchable-rubber-based (SR-based) triboelectric nanogenerator (TENG) is developed that can not only harvest energy but also serve as self-powered multifunctional sensors. It consists of a layer of elastic rubber and a layer of aluminum film that acts as the electrode. By stretching and releasing the rubber, the changes of triboelectric charge distribution/density on the rubber surface relative to the aluminum surface induce alterations to the electrical potential of the aluminum electrode, leading to an alternating charge flow between the aluminum electrode and the ground. The unique working principle of the SR-based TENG is verified by the coupling of numerical calculations and experimental measurements. A comprehensive study is carried out to investigate the factors that may influence the output performance of the SR-based TENG. By integrating the devices into a sensor system, it is capable of detecting movements in different directions. Moreover, the SR-based TENG can be attached to a human body to detect diaphragm breathing and joint motion. This work largely expands the applications of TENG not only as effective power sources but also as active sensors; and opens up a new prospect in future electronics.

1. Introduction

Recently, the triboelectric nanogenerators (TENGs), which operate based on the conjunction of triboelectrification and electrostatic induction,[1] have attracted extensive attention due to their advantages of efficiently harvesting ubiquitous mechanical energies and serving as self-powered active sensors to detect pressure, acoustic waves, chemicals, motion, etc. Up to date, four fundamental working modes for the TENGs have been developed to accommodate various types of mechanical motion, namely the vertical contact-separation mode, the in-plane sliding mode, the single-electrode mode, and the freestanding triboelectric layer mode.[2–13] However, in those working modes, the geometric deformation of the triboelectric layer is not taken into account and the triboelectric charge density is considered as constant, which may not be applicable in certain cases. In addition, the fast development of portable and personal electronics requires devices to be wearable, scalable, and low cost. Lately, the stretchable electronics that enable applications on rugged surface and moveable parts have come into the way of overcoming the limitations of rigid substrates and planar formats, and promoted the development of wearable electronics.[14–20] Still, the development of stretchable/wearable power generation devices is highly desirable.

In this paper, we introduce a new type of stretchable-rubber-based (SR-based) TENG that is based on the triboelectrification and electrostatic induction between a piece of stretchable rubber and an aluminum film, which is a potential approach as a power source for stretchable electronics. The SR-based TENG exploits the shape/length expansion rather than the position shift of the rubber, which induces an in-plane charge separation and results in a potential difference between the aluminum electrode and the ground. In this way, an alternating output current can be produced by periodically stretching and releasing the rubber. This unique working principle of TENG was further confirmed by numerical calculations and controlled experiments. The investigations on the parameters influencing the output performance of the SR-based TENG indicated possible approaches to optimize its output power as well as its potential applications as self-powered motion sensors. On the basis of its motion sensing capability and the high elasticity of the rubber, the SR-based TENG can be mounted onto a human body; and a self-powered health monitoring system could be realized for detections of physiological activities and joint movements. This work provides new design opportunities for TENGs with great

F. Yi, Dr. Q. Liao, Prof. Y. Zhang
State Key Laboratory for Advanced Metals and Materials
School of Materials Science and Engineering
University of Science and Technology Beijing
Beijing 100083, China
E-mail: yuezhang@ustb.edu.cn
F. Yi, Dr. Q. Liao, Prof. Y. Zhang
Key Laboratory of New Energy Materials and Technologies
University of Science and Technology Beijing
Beijing 100083, China
F. Yi, L. Lin, S. Niu, P. K. Yang, Dr. Z. Wang, J. Chen,
Y. Zhou, Dr. Y. Zi, Dr. J. Wang, Prof. Z. L. Wang
School of Materials Science and Engineering
Georgia Institute of Technology
Atlanta, GA 30332-0245, USA
E-mail: zlwang@gatech.edu
Prof. Z. L. Wang
Beijing Institute of Nanoenergy and Nanosystems
Chinese Academy of Sciences
Beijing 100083, China

DOI: 10.1002/adfm.201500428

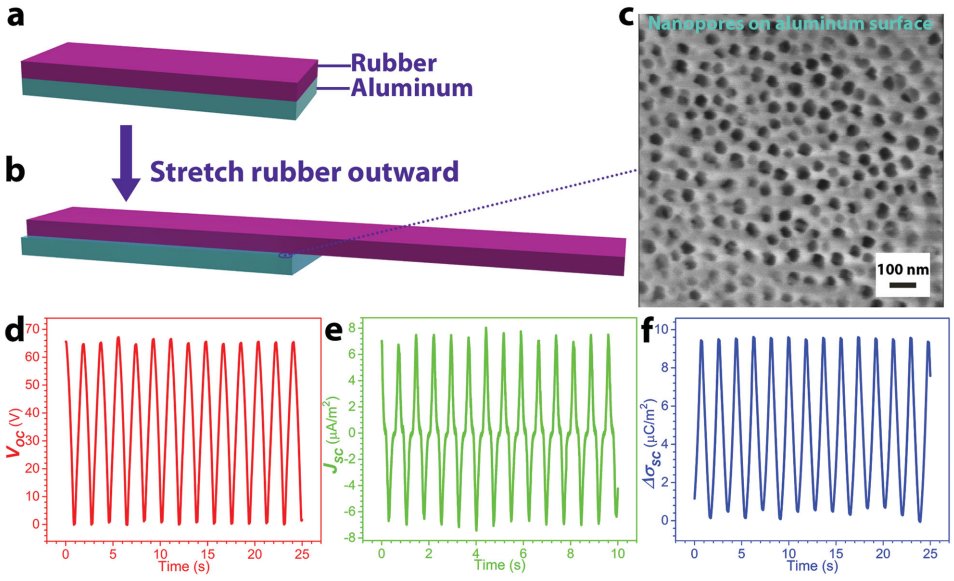

Figure 1. Device Structure and typical electrical output performance of the SR-based TENG. a) Schematic diagram of the SR-based TENG. b) Schematic description of the SR-based TENG with the rubber stretched outward. c) SEM image of the nanopores on the aluminum film. d–f) The measured typical electrical signals by stretching the rubber outward and releasing backward: d) the open-circuit voltage (V_{oc}); e) the current density (J_{sc}); f) the transferred charge density ($\Delta\sigma_{sc}$). Note: V_{oc} and $\Delta\sigma_{sc}$ were measured at a velocity of 20 cm s^{-1} within a 160 mm displacement, while the J_{sc} was measured at an acceleration/deceleration of 9 m s^{-2} within a 160 mm displacement.

potential for applications in robotics, entertainment, sports, medical diagnosis, medical treatment, and so on.

2. Results and Discussion

Figure 1a,b show schematic descriptions of the SR-based TENG, which consists of a layer of 200 μm-thick rubber on the top and a layer of 50 μm-thick aluminum foil at the bottom. The aluminum film plays dual roles of a triboelectric surface and an electrode, and its surface was etched by an anodization method to create nanoporous structures (Figure 1c). As demonstrated in previous works, the nanoporous structures on the aluminum surface can increase the effective contact area and thereby enhance the performance of the TENG.[21,22] If the rubber is stretched outward and released inward, electrical signals will be generated. Figure 1d–f exhibit the typical electrical output signals (V_{oc}: ≈65 V; J_{sc}: ≈7.5 μA m^{-2}; $\Delta\sigma_{sc}$: ≈9 μC m^{-2}) of the SR-based TENG with the rubber and aluminum having the same dimension of 30 mm × 88 mm. The fabrication process and measurement setup for the SR-based TENG are elaborated in the Experimental Section. A controlled experiment was also carried out to verify that the noise signal from the movement of the linear motor can be ignored as compared with the electrical output generated when stretching the rubber (Figure S2, Supporting Information).

The operating mechanism of the SR-based TENG is illustrated in **Figure 2**a. Since the rubber and the aluminum film have different abilities to attract electrons, a transfer of surface charge occurs when the two are brought into contact. Specifically, electrons will transfer from the aluminum surface to the rubber surface owing to the fact that the rubber has higher surface electron affinity than the aluminum,[1,23,24] resulting in net negative charges on the rubber and net positive charges on the aluminum. At the original position, the rubber completely overlaps with the aluminum. The negative charges on the rubber nullify the effect of the positive charges on the aluminum, and the aluminum electrode has the same electrical potential as the ground. Once the rubber is stretched outward, there will be an alteration of the distribution of triboelectric charges. On one hand, part of the stretched rubber is out of the overlapped area, which causes an in-plane charge separation and lateral polarization. On the other hand, the decreased charge density on the rubber surface due to the increased surface area leads to reduced negative charges on the part of the rubber within the overlapped area, which also causes an in-plane charge separation. The overall in-plane charge separation will raise the electrical potential of the aluminum electrode in the open-circuit condition, which drives electrons to flow from the ground to the aluminum electrode in the short-circuit condition. Note that the tribocharges on the rubber surface can be preserved for a long period of time in virtue of the nature of insulators;[25] and the total amount of tribocharges remains the same during the stretching process. The rise in the electrical potential of the aluminum electrode and the transfer of charges between the aluminum electrode and the ground will continue until the rubber stops elongating, where both the electrical potential of the aluminum and the amount of transferred charges reach their maximum values. When the rubber is released and moves backward, the separated negative charges on the rubber begin to be counterbalanced by the positive charges on the aluminum and the charge density on the rubber starts to restore. As a result, the electrical potential of the aluminum electrode drops in the open-circuit condition and electrons flow back to the ground in the short-circuit condition. Finally, when the rubber gets back to its original state, the negative charges on

Adv. Funct. Mater. 2015,
DOI: 10.1002/adfm.201500428

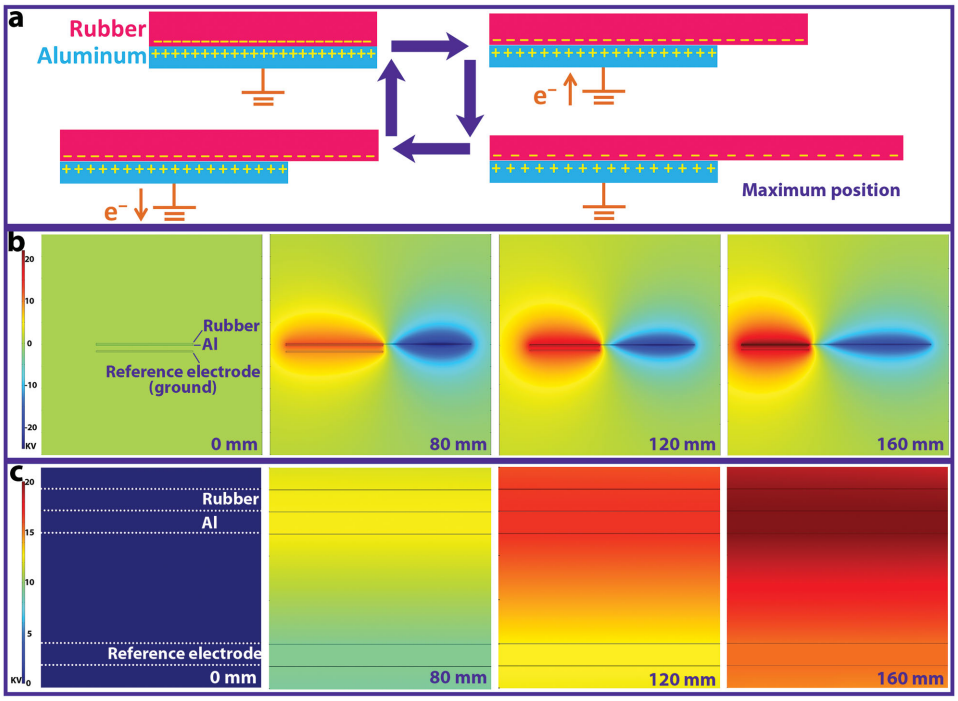

Figure 2. The working mechanism and numerical simulation results of the SR-based TENG using COMSOL. a) Schematic diagram of the working principle of the SR-based TENG. b) The cross-sectional views of the 3D numerical simulation results of the electrical distribution for the SR-based TENG when the rubber is stretched to various magnitudes. c) Enlarged views showing the increasing differences in electrical potential between the aluminum and the ground as the stretched displacement increases. Note: the reference electrode in the simulation model serves as the ground, which will not affect the basic changing trend of output electrical signals.

its surface will be fully offset by the positive charges on the aluminum surface again, and the electric distribution for the SR-based TENG will return to the original status. In this entire operating cycle, an alternating output current is produced as the electrons flow back and forth between the aluminum electrode and the ground, with the zero-crossing of the current curve corresponding to the point where the rubber reaches its maximum stretched displacement. The process of electrostatic induction of this SR-based TENG is different from what were proposed in the preceding works,[4,26–29] and will bring up new insights in the working mode and application of TENGs.

The variations in the electrical potentials and the charge transfer processes of the SR-based TENG can be verified via numerical simulations using COMSOL. The established 3D model has the same structure and dimensions as the real device mentioned above (30 mm × 88 mm × 200 μm for the rubber and 30 mm × 88 mm × 50 μm for the aluminum). The two tribocharged surfaces are assigned with charges of ±100 nC. Note that the amount of initial charges on the triboelectric surfaces will only affect the magnitudes of the calculated electrical potential and transferred charges, and the relative changing trend of the electrical signals will be retained.[30] A reference electrode was set under the aluminum film as the ground, which will not influence the basic changing trend of the electrical signals. Figure 2b presents the cross-sectional view of the 3D numerical simulation results of the electrical potential distribution for the SR-based TENG when the rubber is stretched to various magnitudes (0, 80 mm, 120 mm, and 160 mm). It can be observed that when the rubber and aluminum completely overlap each other, the negative charges on the rubber and the positive charges on the aluminum are fully screened; and when the rubber is stretched outward, the tribocharges are separated. The magnified views in Figure 2c clearly shows the increasing differences in electrical potential between the aluminum and the ground as the stretched displacement increases. It should be noted that when the length of the rubber becomes longer as it is stretched outward, the width and thickness of the rubber will contract, as is schematically depicted in Figure S3 (Supporting Information). The measured changes in the rubber width, the theoretical vertical gaps between the rubber and aluminum, and the differences in the surface charge density of the rubber during the stretching process are shown in Figure S4 (Supporting Information). Although the slight variations in the vertical gap may affect the charge transfer process, its effect is negligible as compared with the in-plane charge separation, which has been verified in a controlled experiment by stretching the rubber within an aluminum film having an area larger than the stretched rubber. As shown in Figure S5 (Supporting Information), little electrical outputs can be observed under the experimental setup.

It has been found that the width of the electrode has a big influence on the performance of the SR-based TENG (**Figure 3**a–d). When the width of the aluminum film is smaller than that of the original rubber, increasing the electrode width leads to an enhancement of both V_{oc} and $\Delta\sigma_{sc}$. However, once the width of the electrode is larger than that of the original

ADVANCED FUNCTIONAL MATERIALS
www.afm-journal.de

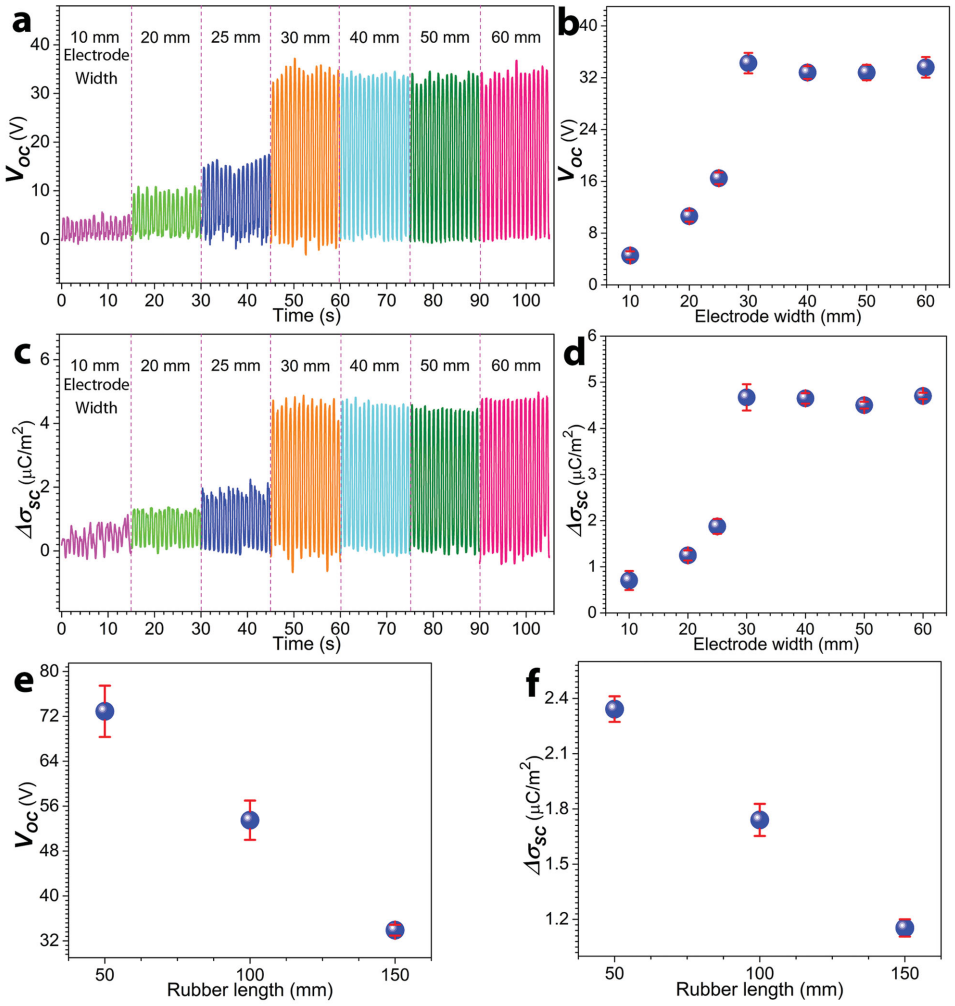

Figure 3. Influences of the electrode width and the rubber length on the electrical signals. The measured a) open-circuit voltage (V_{oc}) and c) transferred charge density ($\Delta\sigma_{sc}$) of SR-based TENGs with different electrode widths. b) The summarized relationship between V_{oc} and the electrode width. d) The summarized relationship between $\Delta\sigma_{sc}$ and the electrode width. Note: the length of the electrode is 88 mm, the size of the rubber is 30 mm × 100 mm (original state), and the stretched displacement is 100 mm. e) V_{oc} and f) ($\Delta\sigma_{sc}$) of SR-based TENGs with different rubber lengths. Note: the size of the electrode is 30 mm × 88 mm, the width of the rubber is 30 mm (original state), and the stretched displacement is 100 mm.

rubber, further enlarging the electrode width will no longer improve the electrical output signals. This is because enlarging the width of the electrode causes an increase in the contact area between the rubber and aluminum; and the maximum contact area comes when the width of the electrode equals to that of the original rubber. It has also been found that when the dimensions of the electrode stay the same, the longer the length of the original rubber, the lower the V_{oc} and $\Delta\sigma_{sc}$ (all the rubber lengths discussed here are longer than that of the electrode), as are presented in Figure 3e,f. The reason for this phenomenon is that the triboelectric charges on the rubber with a longer length will travel a shorter distance outside the overlapped area of the rubber and aluminum, and therefore there will be a reduction in the charge separation between the rubber and aluminum. Additionally, there will be a smaller decrease in the charge density of the rubber with a longer length by the same stretched displacement, which will also result in a decrease in V_{oc} and $\Delta\sigma_{sc}$. Like traditional TENGs, the effective output power of the SR-based TENG depends on the load resistance; and the resistance matching can be used to extract the maximum output power. As shown in Figure S6 (Supporting Information), the SR-based TENG reaches its maximum output power density of ≈76.27 μW m^{-2} at a resistance of ≈2 GΩ. Although compared with the previously reported TENGs, our SR-based TENG showed lower output power; its unique fundamental principle, which can be further applied to other configurations, such as rolling motion, bending motion, and swelling motion,[2,31,32] offers promising options for functional designs in future electronics.

Figure 4 presents the V_{oc} and $\Delta\sigma_{sc}$ of the SR-based TENG when the rubber was stretched to various positions. It can be seen that the measured V_{oc} and $\Delta\sigma_{sc}$ both increase at a decreasing rate as the stretched displacement increases. The measured V_{oc} and $\Delta\sigma_{sc}$ share the same changing trend (Figure S7, Supporting Information), which accords with the general relationship of V_{oc} and $\Delta\sigma_{sc}$ for a TENG:[33–35]

DOI: 10.1002/adfm.201500428

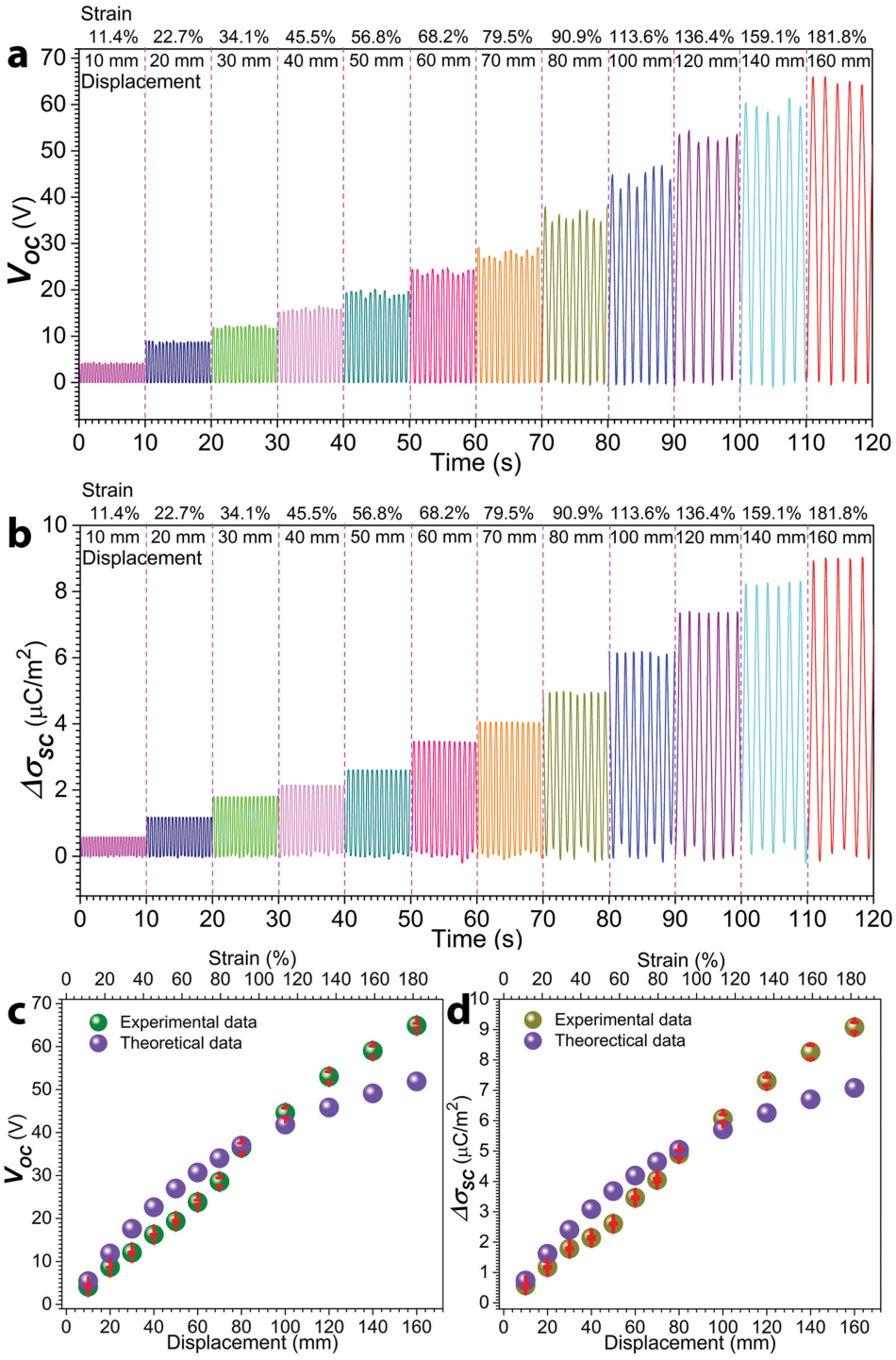

Figure 4. Dependence of the electrical outputs on the stretched displacement/strain. The measured a) open-circuit voltage (V_{oc}) and b) transferred charge density ($\Delta\sigma_{sc}$) under different stretched displacements/strains. c) The summarized relationship between the V_{oc} and the stretched displacement/strain, experimentally and theoretically. d) The summarized relationship between the $\Delta\sigma_{sc}$ and the stretched displacement/strain, experimentally and theoretically.

$$V_{oc} = \Delta\sigma_{sc} \times S \times C^{-1} \quad (1)$$

where S is the area of the electrode, and C is the capacitance between the electrode and the ground for our SR-based TENG, which is a constant. As exhibited in Figure 4c,d, the theoretical predictions of V_{oc} and $\Delta\sigma_{sc}$ from the simulation modeling fit the trend of the experimental data. A slight slower saturate rate of the experimental values can be attributed to the simplifications

made in the analytical derivation and the instrument errors that are hard to remove during the experiments. For example, the slight change in the vertical gap between the rubber and aluminum owing to the shrink in the thickness of the rubber during the stretching was ignored in the simulation model. Note that the actual vertical gap between the rubber and aluminum during the stretching movement is hard to be acquired because the change in the rubber thickness is too much smaller as compared with the lateral dimension and there is an inevitable vertical deviation during the movement due to the motion error of the linear motor. Over a small range of the stretched displacement, there is a nearly linear relationship between the V_{oc} and the stretched displacement; and a displacement resolution of ≈75 μm was obtained by a step motion test with each step of 1 mm (Figure S8a, Supporting Information). The SR-based TENG has a response time of ≈9.1 ms (Figure S8b,c, Supporting Information), which is determined by the resistive-capacitive effects of all the nodes in the whole circuit, including the TENG device and the circuit of the measuring instrument. The SR-based TENG exhibits good reliability and stability in device operation. As shown in Figure S9 (Supporting Information), there is no significant change in electrical output after stretching and releasing the rubber for about 5000 cycles. In addition, since the engineering normal strain is proportional to the stretched displacement:

$$\epsilon = x / L_0 \tag{2}$$

where x is the stretched displacement and L_0 is the original length of the rubber, the SR-based TENG also has the potential capability to predict the applied strains. It should be noted that all of the deformations of the rubber in the experiments are elastic.

If the stretched displacement of the rubber remains the same, changing the velocity or acceleration of the stretching movement will directly influence the current density (J_{sc}), but have almost no effect on V_{oc} and $\Delta\sigma_{sc}$. Figure S10 (Supporting Information) exhibits the velocity–time and displacement–time curves at different velocities and accelerations within the same stretched displacement of 100 mm. As presented in **Figure 5**a,b, the amplitude of the J_{sc} becomes greater as the velocity rises and the peak values can be linearly fitted with an adjusted coefficient of determination of ≈0.994. Similarly, the amplitude of the J_{sc} also enlarges with the increasing acceleration (Figure 5c,d) and is approximately proportional to the square root of acceleration (adjusted coefficient of determination is ≈0.999).

The current density of the SR-based TENG based on single electrode can be written as

$$\begin{aligned} J_{sc} &= \mathrm{d}\Delta\sigma_{sc} / \mathrm{d}t = (\mathrm{d}\Delta\sigma_{sc} / \mathrm{d}x) \times (\mathrm{d}x / \mathrm{d}t) \\ &= (\mathrm{d}\Delta\sigma_{sc} / \mathrm{d}x) \times v \end{aligned} \tag{3}$$

where $\Delta\sigma_{sc}$ is the transferred charge density between the electrode and the ground, x is the stretched displacement, and v is the moving velocity. $\Delta\sigma_{sc}$ can be linearly fitted with the stretched displacement (≤160 mm) with an adjusted coefficient of determination of ≈0.997 (Figure S7b, Supporting Information), hence the term $\mathrm{d}\Delta\sigma_{sc}/\mathrm{d}x$ in Equation (3) can be considered as a constant. For uniform motion, the velocity remains unchanged, thus the amplitude of the J_{sc} will linearly increase with the velocity. For uniformly accelerated motion (symmetric

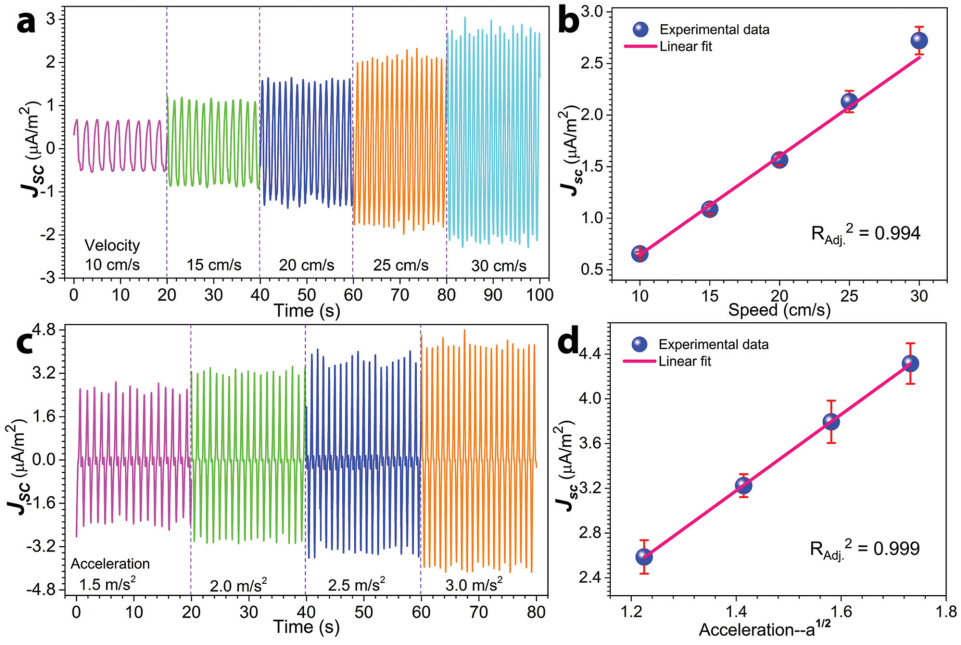

Figure 5. Influences of the stretching velocity and acceleration on the current density (J_{sc}). a) The measured J_{sc} at different velocities. b) Plot of the amplitude of J_{sc} as a function of the velocity, with a linearly fitted relationship. c) The measured J_{sc} at different accelerations. d) The summarized relationship between the amplitude of J_{sc} and the acceleration, with the amplitude of J_{sc} linearly fitted with the square foot of acceleration. Note that the stretched displacement is 100 mm.

Adv. Funct. Mater. 2015,
DOI: 10.1002/adfm.201500428

acceleration and deceleration for the total distance), the J_{sc} reaches its peak value at the maximum velocity:

$$J_{sc-peak} = [(d\Delta\sigma_{sc} / dx) \times v]_{peak} = (d\Delta\sigma_{sc} / dx) \times v_{max} = (d\Delta\sigma_{sc} / dx) \times (2 \times a \times \Delta x)^{1/2} \quad (4)$$

where a is the uniform acceleration and Δx is the covered distance at the acceleration/deceleration phase, which equals to half of the total stretched displacement. Therefore, the amplitude of J_{sc} will have a linear relationship with the square root of the acceleration. Note that the detailed derivation of Equation (4) can be found in the Supporting Information. The V_{oc} and $\Delta\sigma_{sc}$ of the SR-based TENG under different velocities and accelerations are shown in Figure S11 (Supporting Information) and Figure S12 (Supporting Information), respectively. It can be seen that there are almost no changes in V_{oc} and $\Delta\sigma_{sc}$ when increasing the velocity and acceleration. Note that since the inner resistance of the electrometer is not infinitely large, the higher changing rate of $\Delta\sigma_{sc}$ at a larger velocity or acceleration may cause a slight increment in V_{oc} and $\Delta\sigma_{sc}$.

To investigate the potential applications of the SR-based TENG, it has been demonstrated that the SR-based TENGs can be applied to detect moving directions and serve as human motion sensors to detect diaphragmatic breathing and joint action. As exhibited in **Figure 6**, four TENG devices (each device has the same structure and size as the one mentioned in Figure 1) were integrated into a sensor system, with each device connecting to a channel of the multichannel measurement system. The four devices were marked in order from 1 to 4, and each number represents a particular direction. By stretching the rubbers of the devices simultaneously or in certain sequences, it can be seen that the movement in each direction can be recorded separately and accurately in real time without external power source, and the output signals are highly reproducible (Figure 6a–c and Movies 1–3, Supporting Information). Note that the output voltage signal generated when only moving the hand is negligible as compared with the voltage signal from stretching the rubber (Figure S13, Supporting Information).

Figure 7a exhibits the SR-based TENG's application as a self-powered breathing sensor, structured with a piece of aluminum foil (40 mm × 50 mm × 50 μm) at the bottom and a layer of rubber (30 mm × 55 mm × 200 μm) on the top. There was a layer of polytetrafluoroethylene (PTFE) film (thickness: 50 μm) to insulate the aluminum from the human body and the rubber was fixed by a string around the abdomen. It is known that diaphragmatic breathing is the most natural way of breathing. Monitoring the diaphragmatic breathing can get information about the movement of the diaphragm and therefore is very important for diagnosis of disease, medical treatment and postoperative care.[36–38] On inhalation, the diaphragm muscle contracts and pulls downward to increase the volume of the abdomen; while on exhalation, the diaphragm muscle pulls upward to decrease the volume of the abdomen (Figure 7a1,a2).[39] The rubber was at its original state as the stomach reaches the maximum inward position during expiration. As the stomach moves out when starting to breathe in,

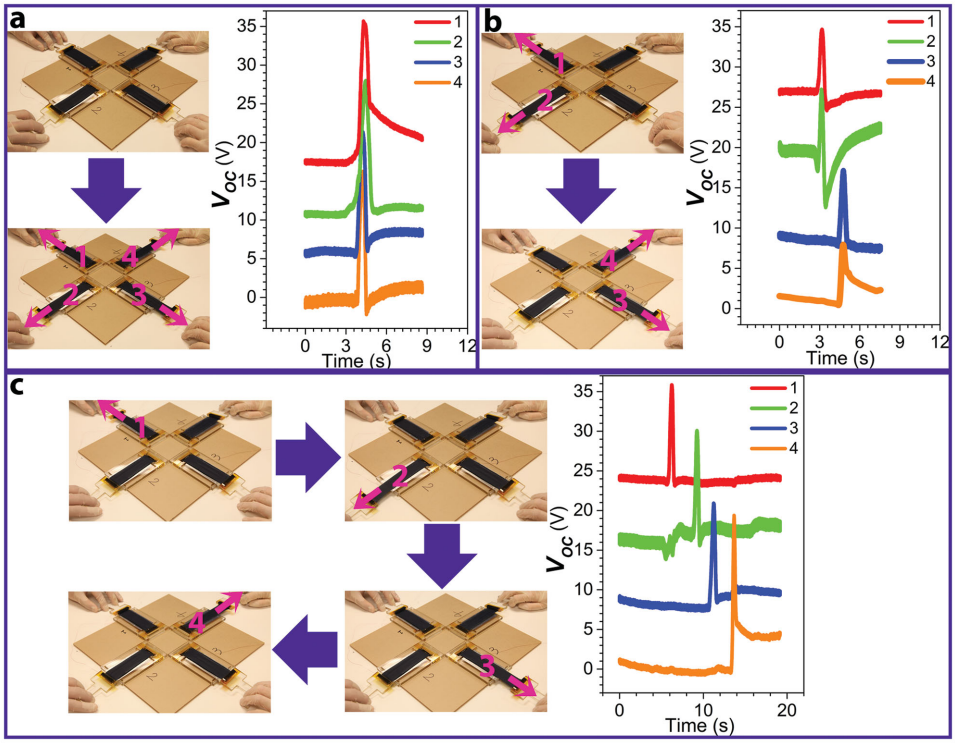

Figure 6. A sensor system through the integration of four SR-based TENG devices to detect directions. a) The measured output voltages when the stretching movements along the four directions happen simultaneously. b) The measured output voltages when there are stretching movements first along directions 1 and 2, then along directions 3 and 4. c) The measured output voltages when the stretching movements along directions 1, 2, 3, and 4 occur in the numerical order.

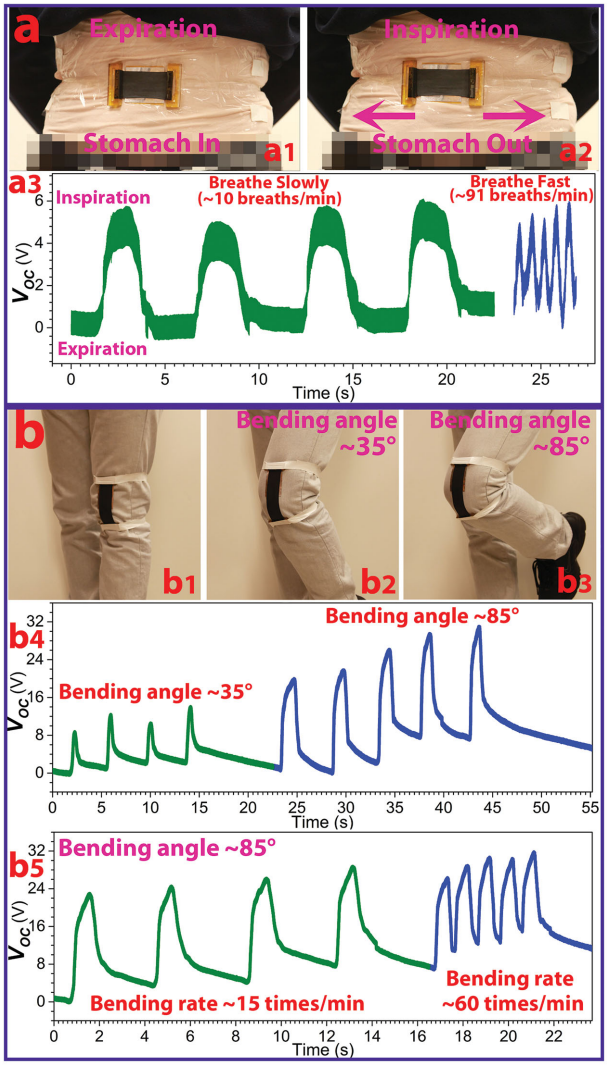

Figure 7. Applications of the SR-based TENG to detect diaphragmatic breathing and joint motion. a) Images and operational data from the breathing sensor: a1,a2) optical images of the device on the abdomen during expiration and inspiration; a3) voltage responses to the diaphragmatic breathing (strain in the rubber: ≈23.96%). b) Images and operational data from the joint motion sensor: b1–b3) optical images of the device on the knee at different bending angles; b4) voltage responses when bending the knee at different angles (strain in the rubber: ≈13.33% at 35°, ≈35.56% at 85°); b5) voltage responses when bending the knee at different rates (bending angle: 85°).

the rubber will be stretched outward due to the increase of the abdominal circumference. The deformation of the rubber will induce a change in the output voltage from the aluminum electrode and hence the breathing process can be monitored (Figure 7a3 and Movie 4, Supporting Information). This working principle could be further applied to detect other physiological activities relating to the tidal of volume such as blood flow and gastrointestinal peristalsis. Human motions involving the movements of joints can also be detected by the SR-based TENG. As presented in Figure 7b, a device (aluminum: 40 mm × 50 mm × 50 µm; rubber: 30 mm × 90 mm × 200 µm) was set over the knee joint. The rubber is stretched when bending the knee and released when straightening the knee, generating output voltage signals. It can be seen that the SR-based TENG is capable of distinguishing the bending angle of the knee (Figure 7b4 and Movie 5, Supporting Information). Moreover, from the recorded voltage signals, the accurate bending rate of the knee can also be acquired (Figure 7b5 and Movie 6, Supporting Information). This idea can be exploited in various areas such as robotics, sports, entertainment, and health care.

3. Conclusion

In summary, we demonstrated a novel type of SR-based TENG that takes advantage of the triboelectrification between a stretchable rubber and an aluminum film. The stretching of the rubber brings about in-plane charge separation between the rubber and aluminum, which induces differences in electrical potential between the aluminum electrode and the ground, driving charges to transfer between the aluminum electrode and the ground. The working principle and the factors that influence the output performance of the SR-based TENG were thoroughly studied. A sensor system was assembled by the SR-based TENG devices to detect moving directions. Furthermore, the SR-based TENG was applied to monitor the diaphragmatic breathing and joint movements of a human body. The basic concepts demonstrated in this paper can be further expanded to construct other configurations so as to harvest multiple forms of mechanical energy and act as functional sensors for detecting various kinds of signals. This work offers new approaches to design electronic devices and initiates applications in ubiquitous electronics.

4. Experimental Section

Materials and Instrumentation: 1) The rubber used in the experiments is a commercial product made by the Qualatex company and the aluminum film was purchased from McMaster-Carr. 2) The morphology of the etched aluminum surface was characterized by a field emission electron microscope (Hitachi SU8010). 3) The output voltage and transferred charges were measured by Keithley 6514 System Electrometer and the output current was measured by Stanford Research SR570. 4) A multichannel system was utilized to measure the output signals for the direction sensor system.

Fabrication of Nanoporous Structures on the Aluminum Surface: 1) An aluminum foil was placed in 3% (mass fraction) oxalic acid ($H_2C_2O_4$) electrolyte for anodization of 5 h, with a platinum plate as the cathode and a bias voltage of 30 V. 2) The obtained alumina layer was etched away in a solution of 20 g L^{-1} chromic acid at 60 °C for 2 h. 3) The aluminum layer was rinsed with distilled water and dried at 50 °C in the air.

Fabrication and Measurement Setup of the SR-Based TENG: 1) The rubber layer was placed on top of the nanostructured aluminum foil. 2) The aluminum foil was mounted onto an acrylic plate. 3) One end of the rubber was fixed on the acrylic plate. 4) The free end of the rubber was connected to a linear motor (Figure S1, Supporting Information). 5) The aluminum foil was connected to the electrical measuring system through a copper wire.

Supporting Information

Supporting Information is available from the Wiley Online Library or from the author.

Adv. Funct. Mater. **2015**,
DOI: 10.1002/adfm.201500428

Acknowledgements

F.Y., L.L., and S.N. contributed equally to this work. The research was supported by National Natural Science Foundation of China (Grant No. 51432005), Beijing City Committee of Science and Technology (Z131100006013004 and Z131100006013005), the Major Project of International Cooperation and Exchanges (2012DFA50990), the Programme of Introducing Talents of Discipline to Universities (B14003), and the National Major Research Program of China (2013CB932602). Fang Yi would like to express her sincere gratitude to the China Scholarship Council (CSC) for the scholarship to help her study in the United States.

Received: February 2, 2015
Revised: March 12, 2015
Published online:

[1] Z. L. Wang, *ACS Nano* **2013**, *7*, 9533.
[2] F.-R. Fan, Z.-Q. Tian, Z. L. Wang, *Nano Energy* **2012**, *1*, 328.
[3] Q. Liang, Z. Zhang, X. Yan, Y. Gu, Y. Zhao, G. Zhang, S. Lu, Q. Liao, Y. Zhang, *Nano Energy* **2015**, DOI: 10.1016/j.nanoen.2014.07.010.
[4] L. Lin, Y. Xie, S. Niu, S. Wang, P.-K. Yang, Z. L. Wang, *ACS Nano* **2015**, *9*, 922.
[5] L. Lin, Y. Xie, S. Wang, W. Wu, S. Niu, X. Wen, Z. L. Wang, *ACS Nano* **2013**, *7*, 8266.
[6] Z.-H. Lin, G. Zhu, Y. S. Zhou, Y. Yang, P. Bai, J. Chen, Z. L. Wang, *Angew. Chem. Int. Ed.* **2013**, *52*, 5065.
[7] S. Wang, S. Niu, J. Yang, L. Lin, Z. L. Wang, *ACS Nano* **2014**, *8*, 12004.
[8] Y. Xie, S. Wang, S. Niu, L. Lin, Q. Jing, Y. Su, Z. Wu, Z. L. Wang, *Nano Energy* **2014**, *6*, 129.
[9] J. Yang, J. Chen, Y. Liu, W. Yang, Y. Su, Z. L. Wang, *ACS Nano* **2014**, *8*, 2649.
[10] Y. Yang, Y. S. Zhou, H. Zhang, Y. Liu, S. Lee, Z. L. Wang, *Adv. Mater.* **2013**, *25*, 6594.
[11] F. Yi, L. Lin, S. Niu, J. Yang, W. Wu, S. Wang, Q. Liao, Y. Zhang, Z. L. Wang, *Adv. Funct. Mater.* **2014**, *24*, 7488.
[12] Y. S. Zhou, G. Zhu, S. Niu, Y. Liu, P. Bai, Q. Jing, Z. L. Wang, *Adv. Mater.* **2014**, *26*, 1719.
[13] G. Zhu, J. Chen, T. Zhang, Q. Jing, Z. L. Wang, *Nat. Commun.* **2014**, *5*, 3426.
[14] M. Kaltenbrunner, M. S. White, E. D. Głowacki, T. Sekitani, T. Someya, N. S. Sariciftci, S. Bauer, *Nat. Commun.* **2012**, *3*, 770.
[15] D.-H. Kim, J.-H. Ahn, W. M. Choi, H.-S. Kim, T.-H. Kim, J. Song, Y. Y. Huang, Z. Liu, C. Lu, J. A. Rogers, *Science* **2008**, *320*, 507.
[16] R.-H. Kim, D.-H. Kim, J. Xiao, B. H. Kim, S.-I. Park, B. Panilaitis, R. Ghaffari, J. Yao, M. Li, Z. Liu, V. Malyarchuk, D. G. Kim, A.-P. Le, R. G. Nuzzo, D. L. Kaplan, F. G. Omenetto, Y. Huang, Z. Kang, J. A. Rogers, *Nat. Mater.* **2010**, *9*, 929.
[17] J. A. Rogers, T. Someya, Y. Huang, *Science* **2010**, *327*, 1603.
[18] T. Sekitani, H. Nakajima, H. Maeda, T. Fukushima, T. Aida, K. Hata, T. Someya, *Nat. Mater.* **2009**, *8*, 494.
[19] T. Sekitani, Y. Noguchi, K. Hata, T. Fukushima, T. Aida, T. Someya, *Science* **2008**, *321*, 1468.
[20] S. Xu, Y. Zhang, L. Jia, K. E. Mathewson, K.-I. Jang, J. Kim, H. Fu, X. Huang, P. Chava, R. Wang, S. Bhole, L. Wang, Y. J. Na, Y. Guan, M. Flavin, Z. Han, Y. Huang, J. A. Rogers, *Science* **2014**, *344*, 70.
[21] P. Bai, G. Zhu, Z.-H. Lin, Q. Jing, J. Chen, G. Zhang, J. Ma, Z. L. Wang, *ACS Nano* **2013**, *7*, 3713.
[22] P. Bai, G. Zhu, Y. Zhou, S. Wang, J. Ma, G. Zhang, Z. L. Wang, *Nano Res.* **2014**, *7*, 990.
[23] A. F. Diaz, R. M. Felix-Navarro, *J. Electrost.* **2004**, *62*, 277.
[24] J. Henniker, *Nature* **1962**, *196*, 474.
[25] F. Saurenbach, D. Wollmann, B. D. Terris, A. F. Diaz, *Langmuir* **1992**, *8*, 1199.
[26] S. Wang, L. Lin, Y. Xie, Q. Jing, S. Niu, Z. L. Wang, *Nano Lett.* **2013**, *13*, 2226.
[27] S. Wang, Y. Xie, S. Niu, L. Lin, Z. L. Wang, *Adv. Mater.* **2014**, *26*, 2818.
[28] Y. Yang, H. Zhang, J. Chen, Q. Jing, Y. S. Zhou, X. Wen, Z. L. Wang, *ACS Nano* **2013**, *7*, 7342.
[29] G. Zhu, C. Pan, W. Guo, C.-Y. Chen, Y. Zhou, R. Yu, Z. L. Wang, *Nano Lett.* **2012**, *12*, 4960.
[30] S. Niu, S. Wang, Y. Liu, Y. S. Zhou, L. Lin, Y. Hu, K. C. Pradel, Z. L. Wang, *Energy Environ. Sci.* **2014**, *7*, 2339.
[31] J.-F. Joanny, F. Jülicher, J. Prost, *Phys. Rev. Lett.* **2003**, *90*, 168102.
[32] L. Lin, S. Wang, Y. Xie, Q. Jing, S. Niu, Y. Hu, Z. L. Wang, *Nano Lett.* **2013**, *13*, 2916.
[33] S. Niu, Y. Liu, S. Wang, L. Lin, Y. S. Zhou, Y. Hu, Z. L. Wang, *Adv. Mater.* **2013**, *25*, 6184.
[34] S. Niu, Y. Liu, S. Wang, L. Lin, Y. S. Zhou, Y. Hu, Z. L. Wang, *Adv. Funct. Mater.* **2014**, *24*, 3332.
[35] S. Niu, S. Wang, L. Lin, Y. Liu, Y. S. Zhou, Y. Hu, Z. L. Wang, *Energy Environ. Sci.* **2013**, *6*, 3576.
[36] W. J. Alilain, K. P. Horn, H. Hu, T. E. Dick, J. Silver, *Nature* **2011**, *475*, 196.
[37] W. D. Reid, G. Dechman, *Phys. Ther.* **1995**, *75*, 971.
[38] X. H. T. Wehrens, S. E. Lehnart, S. Reiken, R. van der Nagel, R. Morales, J. Sun, Z. Cheng, S.-X. Deng, L. J. de Windt, D. W. Landry, A. R. Marks, *Proc. Natl. Acad. Sci. U.S.A.* **2005**, *102*, 9607.
[39] F. D. McCool, G. E. Tzelepis, *N. Engl. J. Med.* **2012**, *366*, 932.